Dalton Transactions

PAPER

View Article Online
View Journal | View Issue

Cite this: *Dalton Trans.*, 2014, **43**, 806

Iron–molybdenum-oxo complexes as initiators for olefin autoxidation with O_2†‡

Jan P. Falkenhagen,[a] Christian Limberg,*[a] Serhiy Demeshko,[b] Sebastian Horn,[c] Michael Haumann,[c] Beatrice Braun[a] and Stefan Mebs[a]

Received 27th August 2013,
Accepted 1st October 2013

DOI: 10.1039/c3dt52349g

www.rsc.org/dalton

The reaction between $[(TPA)Fe(MeCN)_2](OTf)_2$ and $[nBu_4N](Cp^*MoO_3)$ yields the novel tetranuclear complex $[(TPA)Fe(\mu\text{-}Cp^*MoO_3)]_2(OTf)_2$, **1**, with a rectangular $[Mo–O–Fe–O–]_2$ core containing high-spin iron(II) centres. **1** proved to be an efficient initiator/(pre)catalyst for the autoxidation of *cis*-cyclooctene with O_2 to give cyclooctene epoxide. To test, which features of **1** are essential in this regard, analogues with zinc(II) and cobalt(II) central atoms, namely $[(TPA)Zn(Cp^*MoO_3)](OTf)$, **3**, and $[(TPA)Co(Cp^*MoO_3)](OTf)$, **4**, were prepared, which proved to be inactive. The precursor compounds of **1**, $[(TPA)Fe(MeCN)_2](OTf)_2$ and $[nBu_4N](Cp^*MoO_3)$ as well as $Cp^*_2Mo_2O_5$, were found to be inactive, too. Reactivity studies in the absence of cyclooctene revealed that **1** reacts both with O_2 and PhIO *via* loss of the Cp* ligands to give the triflate salt **2** of the known cation $[((TPA)Fe)_2(\mu\text{-}O)(\mu\text{-}MoO_4)]^{2+}$. The cobalt analogue **4** reacts with O_2 in a different way yielding $[((TPA)Co)_2(\mu\text{-}Mo_2O_8)](OTf)_2$, **5**, featuring a $Mo_2O_8^{4-}$ structural unit which is novel in coordination chemistry. The compound $[(TPA)Fe(\mu\text{-}MoO_4)]_2$, **6**, being related to **1**, but lacking Cp* ligands failed to trigger autoxidation of cyclooctene. However, initiation of autoxidation by Cp* radicals was excluded *via* experiments including thermal dissociation of Cp^*_2.

1. Introduction

Epoxides are important synthons for commodity and fine chemicals, and hence their synthesis from olefins *via* oxygenation is an important issue in academic and industrial laboratories. Elegant routes have been developed where the oxidation step is catalysed by metals employing, for instance, alkyl hydroperoxides, hypochloride or iodosylbenzene as the oxidants.[1–3] Obviously, from an environmental and economical point of view dioxygen would represent a much more favourable oxidant, as it does not produce any waste products and is rather cheap.

An important class of aerobic oxidation processes consists of autoxidation reactions. Due to the presence of several different strong oxidants in autoxidation reactions and the multitude of different possible reaction pathways and products, usually autoxidation is considered as a process that has to be suppressed. However, autoxidation reactions may also be utilised on purpose for the aerobic epoxidation of olefins. Even industry pursues corresponding approaches, although the selectivity that can be reached is clearly determined by the substrate. Important industrial scale processes include the oxidation of *p*-xylene to terephthalic acid ($44\ Mt \cdot a^{-1}$), the oxidation of cyclohexane to cyclohexanol and cyclohexanone ($6\ Mt \cdot a^{-1}$) and the production of ethylbenzene hydroperoxide ($6\ Mt \cdot a^{-1}$).[3] Generally the autoxidation of hydrocarbons is assumed to proceed *via* a branched radical chain reaction[4] and while the chain mechanism has been deeply explored in the past, the processes by which the chain reactions may be initiated still receive attention.[5–7] Autoxidation initiation by direct reaction of unactivated hydrocarbons with molecular dioxygen (reactions 1 and 2) is both thermodynamically and kinetically unfavourable[2] and therefore rarely observed.[8]

$$R–H + O_2 \rightarrow R^\bullet + HOO^\bullet \quad (1)$$

$$R–H + O_2 + H–R \rightarrow R^\bullet + HOOH + R^\bullet \quad (2)$$

This is usually circumvented by the use of initiators, typically aliphatic azo compounds, dialkyl peroxides or samples of the corresponding hydroperoxides.[1,2] Once initial peroxyl or alkyl radicals have been formed (reactions 1 and 2), the chain

[a]*Institut für Chemie, Humboldt-Universität zu Berlin, Brook-Taylor-Straße 2, 12489 Berlin, Germany. E-mail: christian.limberg@chemie.hu-berlin.de; Fax: +49 30 2093 6966; Tel: +49 30 2093 7382*
[b]*Institut für Anorganische Chemie, Georg-August-Universität Göttingen, Tammannstraße 4, 37077 Göttingen, Germany*
[c]*Fachbereich Physik, Freie Universität Berlin, 14195 Berlin, Germany*

† Electronic supplementary information (ESI) available: NMR spectra and details on the T_1 relaxation time measurements of **1** and **4**, UV/VIS spectra of the isolated compounds, experimental details on XAS measurements for solutions of **1** and **1**/O_2, crystallographic data and figures depicting the molecular structures of the cations of **2**·$(MeCN)_2$, **3**, **4**·$(MeCN)_2$, and Mößbauer data for **1**. CCDC 936995–936999, 937040. For ESI and crystallographic data in CIF or other electronic format see DOI: 10.1039/c3dt52349g

‡ Dedicated to Professor Dr Peter Comba on the occasion of his 60th birthday.

reactions propagate through trapping of molecular dioxygen by the latter (see reaction 3), while the former can abstract a hydrogen atom from an unactivated hydrocarbon to give an alkyl hydroperoxide and an alkyl radical (reaction 4). Decomposition (reaction 5) generates new radicals which cause branching of the chain reaction.

$$R^{\bullet} + O_2 \rightarrow ROO^{\bullet} \quad (3)$$

$$R\text{–}H + ROO^{\bullet} \rightarrow R^{\bullet} + ROOH \quad (4)$$

$$ROOH(ROOR) \rightarrow RO^{\bullet} + HO^{\bullet}(RO^{\bullet}) \quad (5)$$

In olefin autoxidations there are additional possibilities for chain reaction propagation: alkyl peroxide species can either abstract hydrogen atoms from the α-allylic position of olefins (reaction 6) or add to double bonds leading to the formation of epoxides (reactions 7 and 8) or polyperoxides (reaction 9).[2]

$$ROO^{\bullet} + HCR_2\text{–}CR{=}CR_2 \rightarrow RO_2H + {}^{\bullet}CR_2\text{–}CR{=}CR_2 \quad (6)$$

$$ROO^{\bullet} + C{=}C \rightarrow RO_2\text{–}CR_2\text{–}CR_2{}^{\bullet} \quad (7)$$

$$RO_2\text{–}CR_2\text{–}CR_2{}^{\bullet} \rightarrow RO^{\bullet} + \text{epoxide} \quad (8)$$

$$RO_2\text{–}CR_2\text{–}CR_2{}^{\bullet} + O_2 \rightarrow RO_2\text{–}CR_2\text{–}CR_2\text{–}OO^{\bullet} \quad (9)$$

Typical autoxidation "catalysts" enhance the rate of radical generation by formation of metal–alkyl hydroperoxide complexes, which subsequently undergo homolytic unimolecular decomposition to generate alkylperoxy (reaction 11) and alkoxy radicals (reaction 10) initiating radical chain reactions in the process.[2,9–12]

$$ROOH + M^{(n-1)+} \rightarrow RO^{\bullet} + M^{n+} + OH^{-} \quad (10)$$

$$ROOH + M^{n+} \rightarrow ROO^{\bullet} + M^{(n-1)+} + H^{+} \quad (11)$$

This contribution focuses on radical chain initiation with O_2: we report an iron–molybdenum-oxo complex which triggers autoxidation of cyclooctene, as an exemplary hydrocarbon, by initial activation of O_2 and thus complements the few systems reported in this context so far.[13–15]

2. Results and discussion

In recent years, we have been interested in molecular heterobimetallic oxo compounds that can mimic certain structural units proposed to occur on the surfaces of corresponding heterogeneous catalysts composed of two metal oxide components.[16–22] The fact that MoO_3/Fe_2O_3 catalysts are employed for the oxidation of methanol to formaldehyde in the so-called FORMOX process has spurred us to investigate Fe–O–Mo compounds. While some purely inorganic polyoxometal aggregates[23–30] and coordination polymers[30–37] featuring Fe–O–Mo entities have been published, so far only five structurally characterised molecular coordination compounds have been reported, where molybdate units are bridging ligated iron ions.[27,38–43] Since the replacement of purely inorganic molybdate by a monovalent organomolybdate, namely $Cp^*MoO_3^-$ ($Cp^* = \eta^5\text{-}C_5Me_5$), has already served us for the preparation of model compounds in the past,[16–18] we were interested in an investigation on $(L)Fe^{II}/Cp^*MoO_3^-$ (L = ligand molecule) systems.

Hence, $[(TPA)Fe](OTf)_2$ (TPA = tris(2-pyridylmethyl)-amine, OTf = trifluoromethanesulfonate) was reacted with $[nBu_4N](Cp^*MoO_3)$ in acetonitrile (Scheme 1) resulting in an immediate colour change from yellow to red-brown. After reduction of the volume, layering of the solution with diethyl ether led to red-brown crystals of $[(TPA)Fe(\mu\text{-}Cp^*MoO_3)]_2(OTf)_2(MeCN)_2$ (**1**·$(MeCN)_2$, Fig. 1), which were suitable for structure determination by single crystal X-ray crystallography.

1·$(MeCN)_2$ crystallises with two independent molecules in the asymmetric unit. In the molecular structure of **1**·$(MeCN)_2$ two $[(TPA)Fe]^{2+}$ fragments are bridged by two bidentate $Cp^*MoO_3^-$ ligands, resulting in an eight-membered macrocyclic structure, in which alternating iron-oxo and molybdenum-oxo units [Mo–O–Fe–O–]$_2$ form a bent rectangle (torsion angles as measured for Fe1, Mo1, Mo2, Fe2 −143.17(2)/−145.45(2)°). The iron centres are coordinated by TPA, Mo=O (Fe···O(2,4,7,9) 2.120(4)–2.153(4) Å) and Mo–O$^-$ (Fe–O(1,3,8,10) 1.962(4)–1.968(4) Å) functional groups in a distorted octahedral manner. The corresponding N–Fe–N angles are considerably smaller than those of the precursor $[(TPA)Fe(MeCN)_2](OTf)_2$[44] as the latter is a low-spin complex, where the iron(II) ion has a smaller radius than the high-spin iron(II) centre in **1**. Compared to the typical lengths of molybdenum–oxygen double bonds of 1.69(2) Å, like in $Cp_2^*Mo_2O_5$[45] all Mo=O bonds are significantly lengthened, extending to 1.725(4)–1.731(4) Å for the non-coordinating Mo=O groups and to 1.749(4)–1.757(4) Å for the molybdenum oxido units, whose oxygen atoms are additionally coordinated to an iron

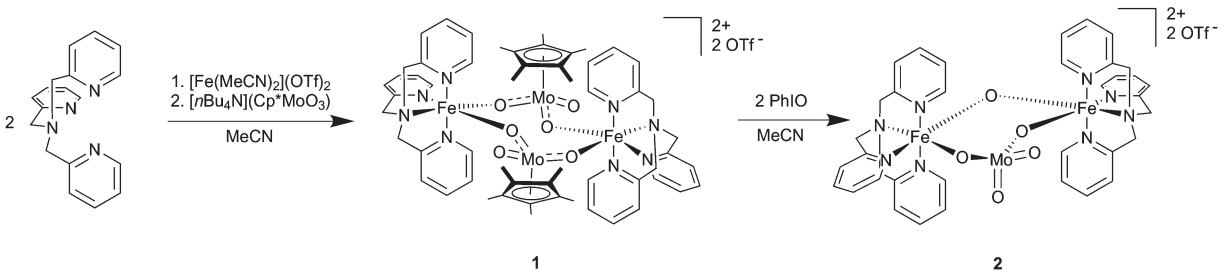

1 2

Scheme 1 Synthesis of $[(TPA)Fe(\mu\text{-}Cp^*MoO_3)]_2(OTf)_2$ (**1**) and $[((TPA)Fe)_2(\mu\text{-}MoO_4)(\mu\text{-}O)](OTf)_2$ (**2**).

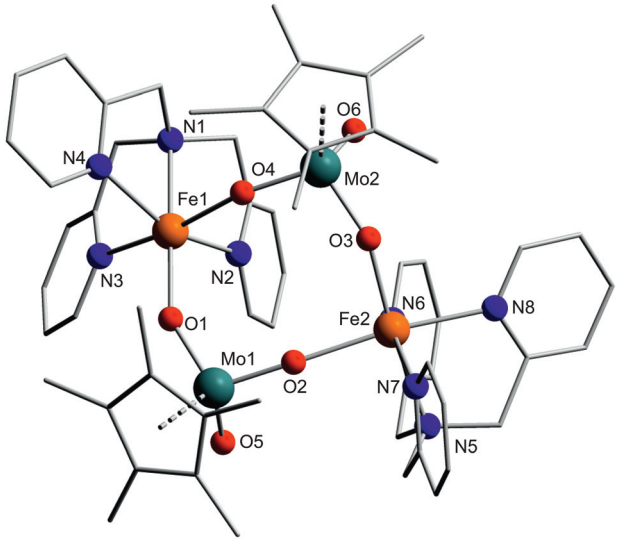

Fig. 1 Molecular structure of the cation of one of the two independent molecules of **1** in the single crystal unit cell. Hydrogen atoms, triflate anions and co-crystallised solvent molecules have been omitted for clarity. Selected bond lengths (in Å) and angles (in °): Mo═O(5,6,11,12) 1.729(4), 1.731(4), 1.728(4), 1.725(4), Mo═O(2,4,7,9) 1.749(4), 1.756(4), 1.757(4), 1.756(4), Mo–O(1,3,8,10) 1.798(3), 1.788(4), 1.788(4), 1.788(4), Fe–O(1,3,8,10) 1.962(3), 1.967(4), 1.968(5), 1.968(4), Fe···O(2,4,7,9) 2.120(4), 2.153(4), 2.121(4), 2.138(4), Mo(1,2,3,4)–C_g 2.115(2), 2.1168(19), 2.115(2), 2.113(2), O–Fe(1,2,3,4)–O 94.20(14), 93.19(14), 96.03(15), 94.05(16), O–Mo(1,2,3,4) = $O_{(coord)}$ 107.33(16), 107.60(16), 106.98(18), 107.23(18), Fe–O(1-4,7-10)–Mo 150.7(2), 164.3(2), 150.0(2), 155.8(2), 160.2(2), 157.2(2), 159.6(2), 153.1(2). C_g = calculated centre of gravity of the Cp*-ligands.

centre. In contrast, the Mo–O (1.788(4)–1.798(4) Å) bonds are considerably shorter than single bonds like those in $Cp_2^*Mo_2O_5$ (1.855(6)–1.894(4) Å).[45] This can be rationalised by the fact that $Cp_2^*Mo_2O_5$ contains common Mo–O–Mo units while Fe–O–Mo═O···Fe moieties are formally present in **1**, the partial delocalisation of which leads to Fe–O···Mo···O– entities.[16,17,46] The measured magnetic moment for compound **1** in solution at 293 K (μ_{eff} = 7.18 μ_B), as determined by the Evans method, is in accordance with the spin only (s.o.) value of two uncoupled h.s. iron(II) centres with total spin quantum numbers of $S1 = S2 = 2$ ($\mu_{s.o.}$ = 6.94 μ_B). A Mößbauer measurement (Fig. S18†) of solid **1** at 80 K supports this interpretation showing only one species with values typical of iron(II) h.s. (I.S. 1.13, Q.S. 2.69). Also, neither Fe^{III} nor Mo^{V} species were detected by investigating solid or dissolved (in acetonitrile, dichloromethane) samples of **1** by X-band EPR spectroscopy. The ^{1}H NMR spectrum of **1** in acetonitrile-d_3 at 300 K and 300.1 MHz features paramagnetically shifted signals in the region from 8.7 ppm to 141.1 ppm as can be expected for a h.s. iron(II) complex (Fig. S6, S7†).[44,47–51] The number of signals exhibited by the TPA ligand indicates an effective 3-fold symmetry in solution and thus a fluxional behaviour on the time scale of the NMR experiment. The observed signals are severely broadened showing line widths ranging from 60 to 1550 Hz. In dichloromethane-d_2 even larger line broadening is observed extending to 3200 Hz for the signals of the methylene groups. The peak assignment was deduced from peak integration, observed line widths and T_1 relaxation measurements:[47,48,52] based on the strong paramagnetic shift, its integral and relative broadness, the signal at the lowest field with a shift of 141.1 ppm ($\Delta\nu_{1/2}$ = 1550 Hz) was assigned to the pyridyl α protons. These are closest to the high-spin metal ion (3.24 Å) and, consistently the T_1 (T_1 measurements at 500.1 MHz and 296 K, Table S2†) determined, was 0.2 ms. The intense broad signal at 55.7 ppm ($\Delta\nu_{1/2}$ = 1200 Hz) also shows a very fast T_1 relaxation (0.4 ms) which again is due to the close proximity of the respective protons to the metal centre and thus points to an assignment to the methylene groups. Relatively sharp features at 47.1 ($\Delta\nu_{1/2}$ = 125 Hz, T_1 = 3.0 ms), 44.8 ($\Delta\nu_{1/2}$ = 90 Hz, T_1 = 4.2 ms) and 25.5 ($\Delta\nu_{1/2}$ = 65 Hz, T_1 = 10.4 ms) are observed for more distant β' (5.03 Å), β (5.20 Å) and γ (5.88 Å) protons; the signal with the smallest chemical shift at 8.7 ppm ($\Delta\nu_{1/2}$ = 120 Hz, T_1 = 3.7 ms) stems from the Cp*-methyl groups. These experimentally determined T_1 values favourably agree with those predicted using the Solomon equation.[51–53] Due to the large Fe···Fe distance in **1**, calculations considering the effect of the distant paramagnetic iron centre do not show a significant effect on the longitudinal relaxation time. However, the typical pattern of downfield shifts attenuating in the order α, β, γ-H observed here has been linked to a predominant σ delocalization mechanism of unpaired spin density[54] and thus a distorted octathedral coordination sphere around the metal centre hinting at a structure of **1** in solution that corresponds to the one in Fig. 1.[44,49,50,52]

Unlike the parent complex $[(TPA)Fe(MeCN)_2](OTf)_2$, **1** proved to be reactive towards dioxygen in solution, which led us to investigate whether **1** could be employed in the selective oxygenation of model substrates, most notably *cis*-cyclooctene. The results showed that the (yet unidentified) primary product of the reaction between **1** and O_2 initiates autoxidation of cyclooctene.

cis-Cyclooctene autoxidation

Typically olefin autoxidation experiments are conducted with high concentrations or even a neat substrate as the solvent.[1,2] To study subtle effects, here low concentrations were favoured that concomitantly decrease reaction rates and yields. In a typical experiment a solution of a certain amount of **1**, *cis*-cyclooctene, and an internal standard in acetonitrile were heated to 80 °C and the atmosphere was replaced by approximately 1.2 bar of pure dioxygen. Samples were collected periodically, freed from metal ions by means of chelex complexation, filtrated over celite and subjected to GC-FID analysis. This proved selective oxidation of cyclooctene to give cyclooctene epoxide (COE, Fig. 2, see Fig. S2† for a GC chart). Investigating the kinetics of this reaction, several aspects of the observed behaviour were not explicable under the assumption of a classical metal-catalysed oxidation reaction. All of the conducted experiments of cyclooctene epoxidation showed S-shaped yield *vs.* time curves hinting towards an initial reaction step forming the active oxidant and/or catalyst in solution. Also, the initial reaction rate did not show a linear correlation

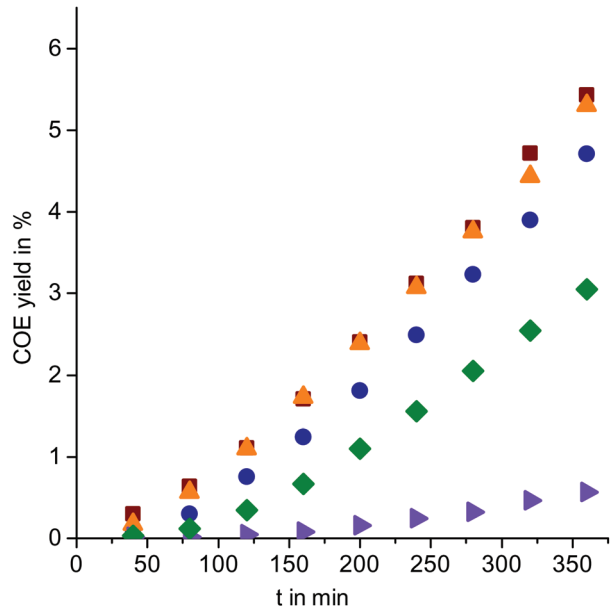

Fig. 2 Yield of cyclooctene autoxidation *vs.* time at 80 °C. Cyclooctene (7.7 mmol), acetonitrile (12 mL), O_2 (1.2 bar), diphenyl ether (70 μmol): ■ 3.5 μmol **1**, ▲ 1.75 μmol **1**, ● 0.875 μmol **1**, ◆ 0.438 μmol **1**, ▶ 0.035 μmol **1**.

with the concentration of the presumed catalyst precursor (Fig. 2). Moreover, control experiments showed that similar initial rates and selectivities towards cyclooctene oxide are observed (Fig. 3) if instead of **1** azobisisobutyronitrile (AIBN) is employed, which is a common radical initiator for autoxidation reactions.[1] Thus it became obvious that the observed reaction is in fact the result of free radical mediated autoxidation.

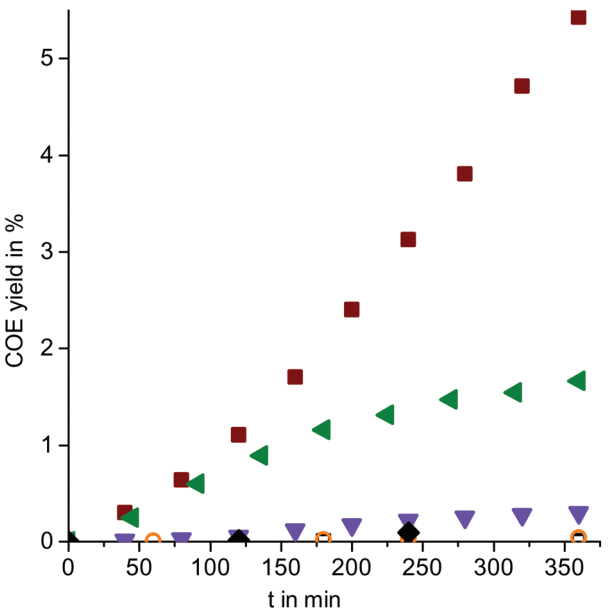

Fig. 3 Yield of cyclooctene autoxidation *vs.* time at 80 °C. Cyclooctene (7.7 mmol), acetonitrile (12 mL), O_2 (1.2 bar), diphenyl ether (70 μmol): ■ 3.5 μmol **1**, ◀ 6.1 μmol AIBN, ▼ 3.5 μmol $Cp_2{}^*Mo_2O_5$, ◆ 7 μmol **3**, □ 7 μmol $[(TPA)Fe(MeCN)_2](OTf)_2$, ○ no catalyst.

Interestingly, the rate of AIBN driven autoxidation drops to a rate similar to that observed with 0.07 μmol **1**, which stresses the efficiency of **1** as a radical chain initiator and also suggests that beyond that it also acts as a (pre)catalyst. Referring to the beginning of this section it should be emphasized at this point that rate and yield can be enhanced dramatically by increasing the substrate concentration (for a demonstration of the effect of adding twice the amount of substrate see Fig. S1†), while the selectivity of the reaction is essentially unaffected (Fig. S2†).

In order to find out how far the potential to initiate autoxidation is a special property of **1**, we have compared the reactivity of the precursors used for the synthesis of **1**, of related $Cp_2{}^*Mo_2O_5$ and related high-spin iron(II) complexes (TPA)-$FeCl_2$ [55] and $[(Tp^{Ph,Me})Fe]Cl$ (Tp = trispyrazolylborato).[12] However, no chain initiation was observed employing $[(TPA)Fe(MeCN)_2](OTf)_2$, $(TPA)FeCl_2$, $[(Tp^{Ph,Me})Fe]Cl$, or $[nBu_4N](Cp^*MoO_3)$, whereas using $Cp_2{}^*Mo_2O_5$ the observed activity was negligible, so that neither ligated iron(II) nor molybdenum entities featuring terminal or bridging oxido ligands can be solely responsible for the observed behaviour.

Therefore we became interested in the nature of the initiating species formed from **1**. Low temperature UV/VIS experiments conducted in acetonitrile (−40 °C), dichloromethane or proprionitrile (−80 °C) solutions did not reveal any labile intermediates and thus did not provide any evidence regarding the nature of the initial **1**/O_2 product.

To evaluate the importance of the iron centres in **1**, we have also reacted $[(TPA)Zn](OTf)_2$ and $[(TPA)Co](OTf)_2$ with $[nBu_4N](Cp^*MoO_3)$, analogous to the synthesis of **1**. This led to the isolation of $[(TPA)Zn(Cp^*MoO_3)](OTf)$ (**3**) and $[(TPA)Co(Cp^*MoO_3)](OTf)$ (**4**) (Scheme 2). Prolonged drying in high vacuum led to the loss of co-crystallised solvent molecules and afforded the analytically pure compounds. In contrast to the molecular structure of **1** within the single crystal, in the molecular structures of both **3**·$(MeCN)_2$ and **4**·$(Et_2O)_{0.5}$·$(MeCN)_{0.5}$ the coordination of only one $Cp^*Mo(O)_2O^-$ unit per 3d-metal centre is observed, leading to slightly distorted trigonal bipyramidal coordination spheres at the central atoms. Both structures are largely similar (Fig. 4 shows the structure of **4**·$(Et_2O)_{0.5}$·$(MeCN)_{0.5}$; for the molecular structure of **3**·$(MeCN)_2$ see Fig. S4†), with only minor differences around the Co/Zn and molybdenum centres. The ^1H NMR spectrum of **4** in acetonitrile-d_3 features a set of signals that is in good agreement with a diamagnetic complex exhibiting a three-fold symmetry in solution. In contrast, the proton NMR spectrum of **4** in the same solvent at 300.1 MHz and 295 K displays a set of broad paramagnetically shifted signals in the region from 144.5 to −0.8 ppm again indicative of a three-fold symmetry for dissolved **4** on the NMR time scale (Fig. S8, S9†). Integrals, linewidth data and T_1 relaxation times were considered to assign the signals to the groups of equivalent protons in **4**. Correct longitudinal relaxation times can be predicted for methylene, α and one of the β proton groups using the Solomon equation (eqn (S1)–(S4), Table S3†), while in contrast to **1** the measured values of the second group of β protons and the γ protons are

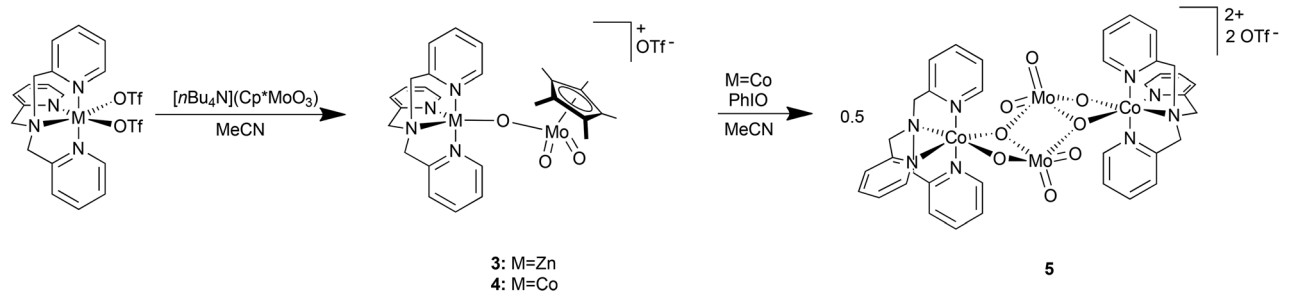

Scheme 2 Synthesis of [(TPA)Zn(Cp*MoO_3)](OTf) (**3**), [(TPA)Co(Cp*MoO_3)](OTf) (**4**), and reaction of **4** with iodosobenzene (PhIO) to give [((TPA)-$Co)_2(\mu\text{-}Mo_2O_8)$](OTf)$_2$ (**5**).

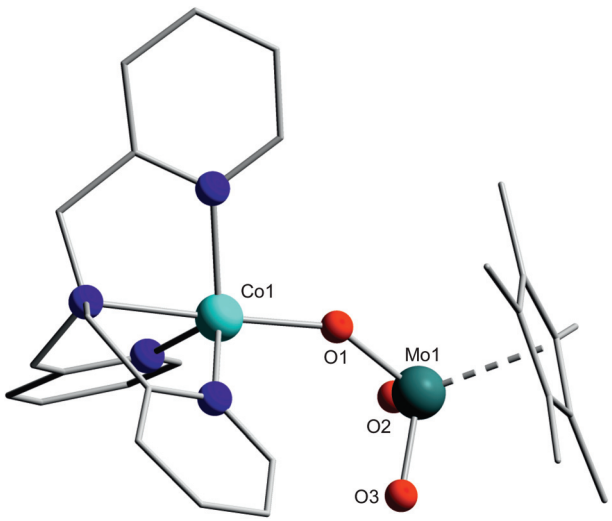

Fig. 4 Molecular structure of the cation of [(TPA)Co(Cp*MoO_3)](OTf) (**4**). Hydrogen atoms, triflate anions and co-crystallised solvent molecules have been omitted for clarity. Selected bond lengths (in Å) and angles (in °): Co1–O1 1.924(6), O1–Mo1 1.809(6), Mo1=O2 1.728(6), Mo1=O3 1.730(6), Mo1–C_g 2.116(4), Co1–O1–Mo1 147.1(3), O1–Mo1–O2 106.2(3), O2–Mo1–O3 105.7(3), O3–Mo1–O1 105.4(3).

much larger than calculated. Hence, the paramagnetic relaxation mechanism does not seem to be dominant in this case. Moreover, due to the smaller line broadening compared to **1** a standard 2D COSY-DQF experiment could be used to identify scalar couplings and thus to establish bond connectivities between the pyridylic β/β′ and γ protons (Fig. S10†).[52,56,57] The characteristic upfield shift of the pyridyl γ-H in metal-TPA complexes has been observed before and interpreted as the effect of a π mechanism superimposed on a dominant σ delocalisation mechanism of unpaired spin density.[50] Since this is only possible in a trigonal pyramidal geometry around the metal centre, NMR indicates that the molecular structure of **4** in the solid state is retained in solution.[44,50,51]

Cyclooctene epoxidation studies conducted for **3** and **4** showed that, under the same conditions as those employed in the case of **1**, neither of these compounds proved to be an initiator for the autoxidation reaction: **4** reacts with dioxygen, but no main oxidation product could be identified. Not surprisingly, **3** does not react at all. Contemplating the functioning of **1** as a radical chain initiator one mechanistic possibility is the initial binding and activation of O_2 between its two iron centres, finally leading to a high valent Fe^{IV}=O species, which triggers radical reactions *via* H atom abstraction or addition to the π bond.[82] The Fe···Fe distance of 5.23 Å should allow to accommodate a peroxide ligand between the iron centres (a simultaneous dissociation of one pyridyl arm should be expected).[58–60] Hence the independent generation of such Fe^{IV}=O species was pursued in the next step employing iodosobenzene (PhIO) as the oxygen atom transfer reagent. For comparison the same reaction was studied for **4**.

1 reacts with iodosobenzene (Scheme 1), formally, losing Cp_2* and MoO_3 to give the known diiron(III) cation [$((TPA)Fe)_2$-$(\mu\text{-}MoO_4)(\mu\text{-}O)]^{2+}$ (**2**, Fig. S3†).[40] In the presence of cyclooctene no chain initiation was observed. According to HR-ESI investigations, $[((TPA)Fe)_2(\mu\text{-}MoO_4)(\mu\text{-}O)]^{2+}$ is also the major final product of the reaction of **1** with O_2. This is further corroborated by molybdenum K-edge XAS measurements for acetonitrile solutions of **1** prior to and after exposition to dioxygen under conditions suitable for cyclooctene autoxidation. For **1**, the Mo K-edge shape, EXAFS spectrum and respective simulation parameters were in agreement with the crystal structure (chapter S4, Table S4 and Fig. S11†), albeit with the typical deviations in bond lengths and angles that occur comparing the molecular structure in solution and in the solid state. They reveal one Mo=O bond (1.74 Å), two Mo–O bonds (1.77 Å), two Mo···Fe distances at 3.45 Å, and pronounced contributions to the spectrum by Mo–C interactions due to the Cp* ring. For **1**/O_2, the K-edge revealed an increased pre-edge feature (at 20 010 eV), which suggested an increased number of Mo=O bonds. In the EXAFS spectrum, Mo–C^{Cp*} contributions were not observed any more and its simulation revealed a first-sphere coordination of the Mo with likely four Mo–O bonds (2×1.70 Å and 2×1.93 Å). The presence of two molybdenum–oxygen distances differing by 0.2 Å explained the diminished FT amplitude of **1**/O_2 compared to **1**, which is due to interference effects. The Mo···Fe distances in **1**/O_2 appear to be slightly shorter compared to **1**. All these observations are in agreement with the formation of **2** as the final product after O_2 treatment of **1** dissolved in acetonitrile. It is stable in air and can thus not account for autoxidation. An intermediate between **1** and **2** formed *in situ* will thus be responsible. The reaction of **4** with PhIO (Scheme 2) proceeds differently from

the one of **1**: it affords the novel compound $[((TPA)Co)_2(\mu\text{-}Mo_2O_8)](OTf)_2$ (**5**, Fig. 5) that features two $[(TPA)Co]^{3+}$ units, bridged by a $Mo_2O_8^{4-}$ unit, which is hitherto unprecedented as a building block of heterometallic coordination compounds. So far it has only been observed bound by additional molybdenum atoms in larger aggregates.[61–64] The τ-value calculated for the coordination spheres of the symmetry equivalent molybdenum atoms is effectively zero indicating perfectly square pyramidal coordination environments.[65] Consequently, the reactions of both **1** and **4** with oxidants led to a loss of the Cp* ligands, probably in the form of Cp*$^{\bullet}$ radicals. Indeed, after the reaction of **4** with PhIO, decamethylbis(cyclopentadienyl) (Cp_2*) was isolated as a byproduct in yields up to 20%, indicating the intermediate formation and recombination of Cp*$^{\bullet}$ radicals. This raised the idea that Cp*$^{\bullet}$, which is known to trap dioxygen leading to peroxyl radicals,[66] might play a role in the initiation of autoxidation. To test the hypothesis that Cp*$^{\bullet}$ radicals are relevant, a further experiment was carried out employing independently synthesised Cp_2*, which was then subjected to thermal dissociation under reaction conditions. However, no chain initiation was observed thus ruling out the involvement of these radicals.[67–69] In this context $((TPA)Fe)_2(\mu\text{-}MoO_4)_2$ (**6**, Fig. S5†) was also synthesised and subjected to test reactions. Over 7 h at 80 °C this did not reveal observable activity, perhaps not surprisingly as **6** is rather similar to **2**. However, from these results it is clear that although Cp*$^{\bullet}$ radicals are not directly responsible for the autoxidation initiation, Cp* nevertheless plays an important role as a spectator ligand governing the initial reactivity of the system.

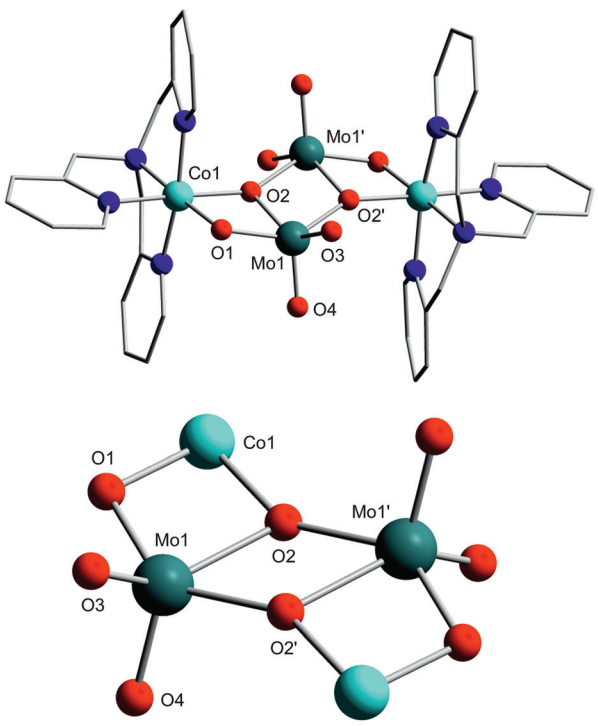

Fig. 5 Molecular structure of the cation of $[((TPA)Co)_2(\mu\text{-}Mo_2O_8)](OTf)_2$ (**5**). Hydrogen atoms, triflate anions and co-crystallised solvent molecules have been omitted for clarity. Selected bond lengths (in Å) and angles (in °): Mo1–O1 1.850(5), Mo1–O2 2.096(5), Mo1–O2′ 1.994(5), Mo1═O3 1.717(5), Mo1═O4 1.712(5), Co1–O1 1.877(5), Co1–O2 1.927(5), O1–Mo1–O2 75.9(2), O1–Mo1–O3 100.3(2), O2–Mo1–O2′ 71.1(2), O2′–Mo1–O3 93.7(2), O1–Mo1–O4 106.3(2), O2–Mo1–O4 110.2(2), O2′–Mo1–O4 103.4(2), O3–Mo1–O4 107.2(3), O2′–Mo1′–Mo1–O2 –180.0(3).

3. Conclusions

From the gathered results we conclude the following:

- **1**/O_2 represents an efficient system for initiating autoxidation.
- **1** is unique with respect to its dioxygen reactivity as compared to the complex metal fragments it was constructed from and also with respect to related iron/molybdenum compounds.
- The presence of iron(II) ions is important as their replacement deactivates the system.
- It follows that dioxygen is activated at one or both of the iron centres within **1**. However, the ultimately formed oxidant is different from the one produced *via* treatment with PhIO, as the latter cannot be used to achieve autoxidation.
- We propose that the oxidizing species formed triggers autoxidation of cyclooctene by H-atom abstraction or π bond addition.

In our future work we will extend these studies to other types of ligands at the iron centres with the aim of gathering further information on the active species and the influence of the organomolybdate on its formation.

4. Experimental details

4.1 General procedures

All manipulations were carried out in a glovebox, or else by means of Schlenk-type techniques involving the use of a dry argon atmosphere. Microanalyses were performed using a Hekatech Euro EA 3000 elemental analyser. Infrared (IR) spectra were recorded using samples prepared as KBr pellets using a Shimadzu FTIR-8400S spectrometer. HR-ESI-MS spectra were collected using an Agilent Technologies 6210 Time-of-Flight LC-MS instrument.

4.1.1 NMR spectroscopy. The NMR spectra were recorded using Bruker DPX 300, Avance III 300 (^{1}H 300.1 MHz) or Avance III 500 (^{1}H 500.1 MHz) NMR spectrometers. Chemical shifts are reported in ppm, relative to residual proton signals of the deuterated solvent (dichloromethane-d_2 at 5.32 ppm, acetonitrile-d_3 at 1.94 ppm, benzene-d_6 at 7.16 ppm), respectively. Measurements to obtain non-selective proton longitudinal relaxation times (T_1) were performed using a standard inversion recovery experiment with a 180°-τ-90°-AQ pulse sequence. To secure the validity of the results, for each sample multiple experiments with different transmitter frequency offsets were carried out. The Bruker Topspin T_1/T_2 module was used to obtain T_1 values in a non-linear fitting procedure.

4.1.2 Crystal structure determination. All data were collected at 100 K with a STOE IPDS 2T diffractometer. The

crystals were mounted on a glass fiber and then transferred into the cold nitrogen gas stream of the diffractometer. In all cases Mo-Kα radiation (λ = 0.71073 Å) was used; the radiation source was a sealed tube generator with a graphite monochromator. The structures were solved by direct methods (SHELXS-97) and refined by full-matrix least squares procedures based on F^2 with all measured reflections (SHELXL-97).[70] All non-hydrogen atoms were refined anisotropically. Hydrogen atoms were introduced in their idealized positions and refined as riding. A multi-scan absorption correction[71] was applied for complex **3**·$(MeCN)_2$ and **4**·$(Et_2O)_{0.5}$·$(MeCN)_{0.5}$ and numerical absorption correction[72] for the other complexes (Table 1).

4.1.3 GC-FID analysis. All autoxidation yields were determined using a Varian 3800-GC equipped with FI and Varian 4000 MS detectors. The samples were injected automatically employing split injectors. The capillary columns used were Varian factor FOUR VF-5 ms or VF-WAXms 30 mm × 0.25 mm respectively. Cyclooctene, cyclooctene oxide and decamethylbis(cyclopentadienyl) were identified by means of their retention times and mass spectra, compared to those of authentic samples of these substances. Cyclooctene oxide and decamethylbis(cyclopentadienyl) were quantified by internal calibration using diphenyl ether as the reference. The stability of the chosen reference was ensured by comparison to naphthalene as a secondary internal reference.

4.1.4 Magnetic susceptibility measurements. Evans method was used to determine the magnetic moments in solution at r.t.[73] The samples were measured in acetonitrile-d_3 with 1% tetramethylsilane (TMS), together with a capillary tube that contained acetonitrile-d_3 with 1% TMS as an internal standard. Different susceptibility measurements led to different shifts of the TMS resonances. For the diamagnetic correction of the susceptibility, Pascal's constants were used.[74]

4.1.5 EPR spectroscopy. X-band EPR spectra were recorded on an ERS 300 (ZWG/Magnettech GmbH, Berlin-Adlershof, Germany) equipped with a quartz dewar for measurements at liquid nitrogen temperature. *g*-Factors were calculated regarding a Cr^{3+}/MgO reference (g = 1.9796).

4.1.6 UV/VIS spectroscopy. UV/VIS data were recorded on an Agilent 8453A diode-array spectrometer using quartz cuvettes equipped with a Unisoku, Japan Unispeks USP-203-A Cryostat providing a controlled temperature environment during measurements.

4.1.7 Materials. TPA,[75] LiCp*,[76] $Fe(MeCN)_2(OTf)_2$,[77] $[(Tp^{Ph,Me})Fe]Cl$,[12] $[(TPA)Fe]Cl_2$,[78] $[nBu_4N](Cp^*MoO_3)$,[79] $Cp_2^*Mo_2O_5$,[46] $[nBu_4N]2(MoO_4)$,[80] and iodosobenzene[81] were prepared according to the literature procedures. CuCl was purchased from Acros Organics, Belgium. $Zn(OTf)_2$ (98%) was purchased from Sigma-Aldrich. Dioxygen N48 was obtained from Air Liquide. Solvents were purified, dried, degassed, and stored over molecular sieves (3 Å) prior to use.

4.1.7.1 Synthesis of 1,1′,2,2′,3,3′,4,4′,5,5′-decamethyl-bis-(cyclopentadienyl) (Cp_2^*). Cp_2^* was synthesised by a modified literature procedure.[69] To a suspension of 0.98 g (10 mmol) CuCl in 40 mL of thf at −78 °C a suspension of 1.42 g LiCp* (10 mmol) in 25 mL of thf was added. The mixture was stirred at that temperature and allowed to slowly warm to r.t. overnight. The reaction mixture was filtered off and the volume of the filtrate was reduced. The residual oil was extracted three times with 7 mL of *n*-hexane. All volatiles were then removed under reduced pressure to give a slightly yellow oil. Addition of

Table 1 Crystal data and experimental parameters for the crystal structure analysis

Compound	**1**·$(MeCN)_2$	**4**·$(Et_2O)_{0.5}$·$(MeCN)_{0.5}$	**5**·$(MeCN)_4$
Formula	$C_{62}H_{72}F_6Fe_2Mo_2N_{10}O_{12}S_2$	$C_{64}H_{79}Co_2F_6Mo_2N_9O_{13}S_2$	$C_{46}H_{48}Co_2F_6Mo_2N_{12}O_{14}S_2$
Fw/(g mol^{-1})	1631.00	1670.22	1480.82
Crystal system	Triclinic	Monoclinic	Monoclinic
Space group	$P\bar{1}$	$P2_1/c$	$C2/c$
a/Å	11.6964(2)	14.1365(4)	24.080(5)
b/Å	20.1465(4)	14.2503(6)	15.135(3)
c/Å	29.0322(5)	37.6652(10)	16.790(3)
α/°	91.626(1)	90	90
β/°	90.650(1)	108.3110(19)	116.26(3)
γ/°	96.328(1)	90	90
V/Å^3	6887.1(2)	7203.4(4)	5488(2)
Z	4	4	4
ρ/(g cm^{-3})	1.573	1.540	1.792
μ(Mo-K$_\alpha$)/mm^{-1}	0.912	0.932	1.213
F(000)	3328	3416	2976
Θ range/°	2.01–27.00	1.54–25.00	3.22–26.00
Refl. coll.	77 931	54 821	46 109
Indep. refl.	29 954	12 263	5399
Compl. to Θ	0.997	0.967	0.994
R_{int}	0.0651	0.1034	0.1093
GoF on F^2	0.990	1.070	0.877
$R_1[I > 2\sigma(I)]$	0.0575	0.0793	0.0568
w$R_2[I > 2\sigma(I)]$	0.1373	0.2010	0.1289
R_1 (all data)	0.0864	0.1018	0.0854
wR_2 (all data)	0.1486	0.2111	0.1326
$\Delta\rho_{max}/\Delta\rho_{min}$/(e Å^{-3})	2.631/−1.325	2.588/−1.456	1.275/−0.948
CCDC	936995	936997	936998

3 mL of *n*-hexane and storing the resulting solution at −80 °C for several days resulted in the formation of slightly yellow crystals, which were isolated by filtration, while cold, to give 840 mg (3.11 mmol, 62%) of Cp_2^*. ^{1}H NMR, δ in ppm, C_6D_6 1.77 (s, 12H), 1.68 (s, 12H), 1.16 (s, 6H).

4.2 Synthesis of [(TPA)Fe(μ-Cp*MoO$_3$)]$_2$(OTf)$_2$ (1)

1.000 g (1.37 mmol) of [(TPA)Fe(MeCN)$_2$](OTf)$_2$ was dissolved in 30 mL of acetonitrile resulting in an orange solution. 0.720 mg (1.37 mmol) of [*n*Bu$_4$N](Cp*MoO$_3$) were then added to this mixture. This was accompanied by an immediate colour change to give a brown solution, which was then concentrated under reduced pressure to about one-third of the original volume. Layering with diethyl ether resulted in the formation of **1**·(MeCN)$_2$ as red-brown crystals, which were suitable for analysis by single crystal X-ray-diffraction. Drying overnight under high vacuum afforded 716 mg (0.46 mmol, 67%) **1** as a brown powder. Elemental analysis, calcd for $C_{58}H_{66}F_6Fe_2Mo_2N_8O_{12}S_2$: C 44.98, H 4.29, N 7.23, S 4.14, found: C 45.04, H 4.19, N 7.10, S 3.88%. IR (KBr) $\tilde{\nu}$ cm^{-1} 3072 vw, 3025 vw, 2916 w, 2859 vw, 1603 m, 1573 w, 1483 w, 1447 m, 1379 vw, 1273 vs, 1264 vs, 1242 s, 1224 m, 1155 s, 1099 w, 1031 vs, 1017 w, 877 s, 836 s, 809 s, 798 vs, 777 s, 768 s, 762 s, 636 vs, 571 vw, 516 w. ^{1}H NMR, δ in ppm, 300 K, CD_3CN 141.1 (br s, 4H, $\Delta\nu_{1/2}$ = 1550 Hz), 55.7 (br s, 10H, $\Delta\nu_{1/2}$ = 1200 Hz), 47.1 (br s, 6H, $\Delta\nu_{1/2}$ = 125 Hz), 44.8 (br s, 6H, $\Delta\nu_{1/2}$ = 90 Hz), 25.5 (br s, 6H, $\Delta\nu_{1/2}$ = 65 Hz), 8.7 (br s, 30H, $\Delta\nu_{1/2}$ = 120 Hz). ^{1}H NMR, δ in ppm, 294 K, CD_2Cl_2 134.3 (br s, 4H, $\Delta\nu_{1/2}$ = 1545 Hz), 70.9 (br s, 8H, $\Delta\nu_{1/2}$ = 3209 Hz), 47.77 (br s, 6H, $\Delta\nu_{1/2}$ = 122 Hz), 44.54 (br s, 6H, $\Delta\nu_{1/2}$ = 100 Hz), 18.68 (br s, 6H, $\Delta\nu_{1/2}$ = 132 Hz), 9.96 (br s, 30H, $\Delta\nu_{1/2}$ = 167 Hz). ^{19}F NMR, δ in ppm, CD_2Cl_2 −63.69.

4.3 Synthesis of [((TPA)Fe)$_2$(μ-O)(μ-MoO$_4$)](OTf)$_2$ (2)

0.164 g (0.745 mmol, 2.1 eq.) of iodosobenzene was added to a solution of 0.550 g (0.355 mmol) of **1** in 100 mL of acetonitrile. The orange solution gradually darkened within minutes to give a red-brown solution while being stirred at r.t. overnight. The solution was then concentrated under reduced pressure to one-fifth of the original volume and 100 mL of diethyl ether were added causing precipitation of a greenish solid. The solid was redissolved in 10 mL of MeCN and again precipitated by addition of 100 mL of diethyl ether (3×) and isolated by filtration which afforded 243 mg (0.208 mmol, 59%) **2** as an olive powder. Crystals which were suitable for X-ray-diffraction analysis were grown by layering a solution of **2** in acetonitrile with diethyl ether. Elemental analysis calcd for $C_{38}H_{36}F_6Fe_2MoN_8O_{11}S_2$: C 39.13, H 3.11, N 9.61, S 5.49, found: C 39.60, H 3.12, N 9.31, S 5.24%. IR (KBr) $\tilde{\nu}$ cm^{-1} 3070 vw, 3034 vw, 2998 vw, 2959 vw, 2925 vw, 2859 vw, 1607 s, 1573 vw, 1485 w, 1441 m, 1384 vw, 1352 vw, 1309 vw, 1275 vs, 1261 vs, 1225 m, 1156 m, 1100 w, 1052 w, 1030 vs, 996 vw, 977 vw, 956 vw, 931 vw, 906 m, 805 m, 784 vs, 734 w, 636 vs, 573 vw, 518 w, 429 w. HR-ESI-MS calcd for $C_{36}H_{36}Fe_2MoN_8O_5$ [**2** − 2(OTf)]$^{2+}$: 435.0275, found 435.0283.

4.4 Synthesis of [(TPA)Zn(Cp*MoO$_3$)]OTf (3)

0.100 g (0.34 mmol) of TPA were dissolved in 20 mL of acetonitrile and 0.125 g (0.34 mmol) of Zn(OTf)$_2$ were then added. The suspension was stirred until all solid was dissolved resulting in a clear colourless solution (30 min). Upon addition of 0.179 g (0.34 mmol) [*n*Bu$_4$N](Cp*MoO$_3$) the solution immediately became yellow in colour. The solution was stirred at r.t. overnight, concentrated to 2 mL under reduced pressure and layered with diethyl ether. After a few days **3**·(MeCN)$_2$ was isolated as yellow crystals which were suitable for analysis by single crystal X-ray-diffraction. Prolonged drying in high vacuum resulted in the loss of the co-crystallised solvent molecules to give 0.227 mg (0.290 mmol, 84%) of **3** as a yellow powder. Elemental analysis, calcd for $C_{29}H_{33}F_3MoN_4O_6SZn$: C 44.43, H 4.24, N 7.15, S 4.09, found: C 44.74, H 4.29, N 7.22, S 4.01%. IR (KBr) $\tilde{\nu}$ cm^{-1} 3110 vw, 3071 vw, 3036 w, 2961 w, 2915 w, 2857 vw, 1610 s, 1573 s, 1437 m, 1377 w, 1319, w, 1267 vs, 1223 m, 1163 s, 1159 s, 1152 s, 1138 s, 1107 w, 1095 vw, 1059 m, 1051 w, 1031 vs, 985 w, 962 w, 883 vs, 856 vs, 805 m, 790 vs, 778 s, 762 s, 753 m, 732 w, 651 w, 637 vs, 629 w, 571 vw, 517 m, 505 w. ^{1}H NMR, δ in ppm, CD_3CN 9.04 (dq, 3H, *J* = 5.4 Hz, *J* = 0.8 Hz), 8.05 (dt, 3H, *J* = 7.8 Hz, *J* = 1.7 Hz), 7.62 (ddd, 3H, *J* = 7.6 Hz, *J* = 5.5 Hz, *J* = 0.8 Hz), 7.52 (dt, 3H, *J* = 7.9 Hz), 4.14 (6H, s, CH_2), 2.05 (s, 15H, CH_3).

4.5 Synthesis of [(TPA)Co(Cp*MoO$_3$)](OTf) (4)

1.000 g (3.44 mmol) TPA were dissolved in 100 mL acetonitrile and 1.229 g (3.44 mmol) Co(OTf)$_2$ were then added. The suspension was stirred for 30 min to give a solution which was deep purple in colour. 1.794 g (3.44 mmol) of solid [*n*Bu$_4$N](Cp*MoO$_3$) were added resulting in a deep green solution which was stirred overnight at r.t. The solution was concentrated to 20 mL. The product was crashed by addition of 100 mL of diethyl ether and the mixture was filtered off using a stainless steel filter cannula. The green solid was redissolved in 20 mL of acetonitrile and layered with diethyl ether which resulted in the formation of green crystals of **4**·(Et$_2$O)$_{0.5}$·(MeCN)$_{0.5}$. Prolonged drying in high vacuum gave 2.460 g (3.16 mmol, 92%) **4** as a green powder. Elemental analysis, calcd for $C_{29}H_{33}F_3MoN_4O_6SCo$: C 44.80, H 4.28, N 7.21, S 4.12, found: C 44.92, H 4.20, N 7.33, S 3.90%. IR (KBr) $\tilde{\nu}$ cm^{-1} 3108 vw, 3067 vw, 3035 vw, 2948 vw, 2915 w, 1609 s, 1573 w, 1485 w, 1435 m, 1375 w, 1314 w, 1267 vs, 1223 m, 1158 s, 1151 s, 1139 m, 1103 w, 1059 w, 1032 vs, 1001 vw, 983 vw, 960 vw, 907 vw, 883 vs, 856 vs, 778 vs, 762 s, 753 m, 733 w, 652 w, 637 vs, 629 w, 572 w, 517 w, 506 w. ^{1}H NMR, δ in ppm, 300.1 MHz, 295 K, CD_3CN 144.5 (br s, 2.3H, $\Delta\nu_{1/2}$ = 820 Hz), 107.3 (br s, 5.2H, $\Delta\nu_{1/2}$ = 660 Hz), 52.7 (br s, 3H, $\Delta\nu_{1/2}$ = 73 Hz), 46.0 (br s, 3H, $\Delta\nu_{1/2}$ = 83 Hz), 11.1 (br s, 15H, $\Delta\nu_{1/2}$ = 52 Hz), −0.8 (br s, 3H, $\Delta\nu_{1/2}$ = 34 Hz).

4.6 Synthesis of [((TPA)Co)$_2$(μ-Mo$_2$O$_8$)](OTf)$_2$ (5)

0.0283 g (0.129 mmol) of iodosobenzene was added to a stirred deeply green solution of 0.100 g (0.129 mmol) **4** in 10 mL of acetonitrile. The resulting suspension was stirred

overnight and within several hours the colour changed to light purple. The mixture was filtered and the filtrate was dried. The purple coloured solid residue was then redissolved in 4 mL of acetonitrile and layered with diethyl ether to give **5**·$(MeCN)_4$ as purple crystals. Drying in high vacuum afforded 49 mg (0.037 mmol, 58%) of **5** as a purple solid. Crystals, which are suitable for analysis by single crystal X-ray diffraction can be grown directly from the reaction mixture by ultrasonication of a suspension of 13.7 mg (0.018 mmol) **4** and 3.9 mg (0.018 mmol) of iodosobenzene in 0.6 mL acetonitrile in a sealed NMR tube followed by storage of respective tube in a horizontal position overnight. Elemental analysis, calcd for $C_{38}H_{36}Co_2F_6Mo_2N_8O_{14}S_2$: C 34.67, H 2.76, N 8.51, S 4.87, found: C 35.10, H 3.10, N 8.12, S 4.26%. IR (KBr) $\tilde{\nu}$ cm^{-1} 3074 vw, 3039 vw, 2961 vw, 2942 vw, 1609 m, 1487 w, 1465 w, 1447 w, 1437 w, 1383 vw, 1276 vs, 1272 vs, 1261 vs, 1224 m, 1158 m, 1113 vw, 1092 vw, 1056 vw, 1030 vs, 997 vw, 923 w, 890 m, 846 w, 821 m, 776 m, 757w, 740 w, 667 m, 660 w, 636 s, 573 w, 518 w, 506 w. ^{1}H NMR, δ in ppm, CD_3CN 8.54 (ps-d, 1H, J = 5.9 Hz), 8.51 (ps-d, 2H, J = 5.7 Hz), 7.91 (td, 2H, J = 7.8 Hz, J = 1.5 Hz), 7.72 (td, 1H, J = 15.5 Hz, J = 1.5 Hz), 7.55 (d, 2H, J = 7.9 Hz), 7.40 (ps-t, 1H, J = 6.1 Hz), 7.29 (ps-t, 2H, J = 6.4 Hz), 7.08 (ps-d, 1H, J = 7.9 Hz), 5.50 (d, 2H, J = 15.9 Hz), 4.78 (s, 2H), 4.69 (d, 2H, J = 16.1 Hz).

4.7 Synthesis of [(TPA)Fe(μ-MoO_4)]$_2$ (6)

To a solution of 290.4 mg (1.00 mmol) of TPA in 10 mL of acetonitrile, 436.1 mg (1.00 mmol) of $[Fe(MeCN)_2](OTf)_2$ were added. The brown solution was stirred for 15 min at r.t. 644.9 mg (1.00 mmol) of $[n Bu_4N]_2(MoO_4)$ were then added causing immediate precipitation of a brown solid. 90 mL of acetonitrile were subsequently added, and the resulting suspension was stirred overnight. After the addition of 100 mL of diethyl ether, the mixture was filtered and the solid residue was dried under high vacuum overnight to afford 388 mg (0.383 mmol, 77%) of **6** as a brown solid. Red crystals of **6**·$(MeCN)_2$ suitable for single crystal X-ray-diffraction analysis were grown by slow diffusion of a solution of 35.5 mg (0.055 mmol) $[n Bu_4N]_2(MoO_4)$ in 4 mL acetonitrile into a solution of 20.0 mg (0.028 mmol) $[(TPA)Fe(MeCN)_2](OTf)_2$ in 8 mL acetonitrile. Elemental analysis, calcd for $C_{36}H_{36}Fe_2Mo_2N_8O_8$: C 42.71, H 3.58, N 11.07, found C 42.49, H 3.53, N 10.95%. IR (KBr) $\tilde{\nu}$ cm^{-1} 3059 vw, 3055 vw, 3016 vw, 2922 vw, 2917 vw, 1601 m, 1570 w, 1478 w, 1456 w, 1441 m, 1391 vw, 1369 vw, 1349 vw, 1311 vw, 1289 vw, 1263 vw, 1152 vw, 1116 vw, 1097 w, 1049 vw, 1015 vw, 996 vw, 979 vw, 903 w, 860 vs, 847 vs, 781 s, 769 s, 660 vw, 636 vw, 621 vw.

Acknowledgements

We are grateful to the Cluster of Excellence "Unifying Concepts in Catalysis" funded by the Deutsche Forschungsgemeinschaft (DFG), and the Humboldt-Universität zu Berlin for financial support. We thank Drs E. Fonda and V. Briois at Samba of SOLEIL for excellent technical support. M.H. thanks the Deutsche Forschungsgemeinschaft for a Heisenberg Fellowship and for funding (grants Ha3265/3-1 and Ha3265/6-1).

References

1 G. Franz and R. A. Sheldon, *Oxidation. Ullmann's Encyclopedia of Industrial Chemistry*, Wiley-VCH Verlag GmbH & Co. KGaA, Weinheim, 7th edn, 2011.
2 R. A. Sheldon and J. K. Kochi, *Metal-Catalyzed Oxidations of Organic Compounds: Mechanistic Principles and Synthetic Methodology Including Biochemical Processes*, Academic Press, New York, 1981.
3 F. Cavani and J. H. Teles, *ChemSusChem*, 2009, **2**, 508–534.
4 N. N. Semenov and G. Wagner, *Einige Probleme der chemischen Kinetik und Reaktionsfähigkeit: (freie Radikale und Kettenreaktionen)*, Akad.-Verl, Berlin, Vom Autor neu bearb. u. autor. Ausg. in deutscher Sprache hrsg. edn, 1961.
5 I. Hermans, J. Peeters and P. A. Jacobs, *Top. Catal.*, 2008, **50**, 124–132.
6 I. Hermans, T. L. Nguyen, P. A. Jacobs and J. Peeters, *ChemPhysChem*, 2005, **6**, 637–645.
7 U. Neuenschwander and I. Hermans, *J. Catal.*, 2012, **287**, 1–4.
8 D. J. Carlsson and J. C. Robb, *Trans. Faraday Soc.*, 1966, **62**, 3403–3415.
9 J. F. Black, *J. Am. Chem. Soc.*, 1978, **100**, 527–535.
10 A. J. Chalk and J. F. Smith, *Trans. Faraday Soc.*, 1957, **53**, 1214–1234.
11 A. J. Chalk and J. F. Smith, *Trans. Faraday Soc.*, 1957, **53**, 1235–1245.
12 T. Tietz, C. Limberg, R. Stößer and B. Ziemer, *Chem.–Eur. J.*, 2011, **17**, 10010–10020.
13 J. P. Hage, J. A. Powell and D. T. Sawyer, *J. Am. Chem. Soc.*, 1995, **117**, 12897–12898.
14 A. Sobkowiak, D. Naróg and D. T. Sawyer, *J. Mol. Catal. A: Chem.*, 2000, **159**, 247–256.
15 D. Naróg, A. Szczepanik and A. Sobkowiak, *Catal. Lett.*, 2008, **120**, 320–325.
16 S. Roggan, C. Limberg, M. Brandt and B. Ziemer, *J. Organomet. Chem.*, 2005, **690**, 5282–5289.
17 S. Roggan, C. Limberg and B. Ziemer, *Angew. Chem., Int. Ed.*, 2005, **44**, 5259–5262.
18 S. Roggan, C. Limberg, B. Ziemer, M. Siemons and U. Simon, *Inorg. Chem.*, 2006, **45**, 9020–9031.
19 S. Roggan, C. Limberg and B. Ziemer, *Angew. Chem., Int. Ed.*, 2005, **117**, 5393–5397.
20 S. Roggan and C. Limberg, *Inorg. Chim. Acta*, 2006, **359**, 4698–4722.
21 C. Knispel, C. Limberg and M. Mehring, *Organometallics*, 2009, **28**, 646–651.
22 C. Knispel and C. Limberg, *Organometallics*, 2011, **30**, 3701–3703.
23 X. Dong, Y. Zhang, B. Liu, Y. Zhen, H. Hu and G. Xue, *Inorg. Chem.*, 2012, **51**, 2318–2324.

24 Y. Zhen, B. Liu, L. Li, D. Wang, Y. Ma, H. Hu, S. Gao and G. Xue, *Dalton Trans.*, 2012, **42**, 58–62.
25 B. Liu, L. Li, Y. Zhang, Y. Ma, H. Hu and G. Xue, *Inorg. Chem.*, 2011, **50**, 9172–9177.
26 D.-L. Long, P. Kögerler, L. J. Farrugia and L. Cronin, *Dalton Trans.*, 2005, 1372–1380.
27 L. Xu, Z. Li, H. Liu, J. Huang and Q. Zhang, *Chem.–Eur. J.*, 1997, **3**, 226–231.
28 J.-Y. Niu, J.-P. Wang, X.-Z. You, T. C. W. Mak and Z.-Y. Zhou, *Polyhedron*, 1996, **15**, 3963–3969.
29 J.-Y. Niu, X.-Z. You and J.-P. Wang, *Transition Met. Chem.*, 1996, **21**, 38–42.
30 A. Müller, S. K. Das, E. Krickemeyer, P. Kögerler, H. Bögge and M. Schmidtmann, *Solid State Sci.*, 2000, **2**, 847–854.
31 J. Zhao, J. Liu, J. Wang and J. Niu, *Chem. Lett.*, 2009, **38**, 474–475.
32 D.-L. Long, P. Kögerler, L. J. Farrugia and L. Cronin, *Chem.–Asian J.*, 2006, **1**, 352–357.
33 P. J. Zapf, R. P. Hammond, R. C. Haushalter and J. Zubieta, *Chem. Mater.*, 1998, **10**, 1366–1373.
34 H.-L. Chen, M.-X. Li, X. He, Z.-X. Wang, M. Shao and S.-R. Zhu, *Inorg. Chim. Acta*, 2010, **363**, 3186–3193.
35 X.-M. Zhang, R.-Q. Fang and S. W. Ng, *Acta Crystallogr., Sect. E: Struct. Rep. Online*, 2004, **60**, m1049–m1050.
36 S. D. Huang and Y. Shan, *J. Solid State Chem.*, 2000, **152**, 229–235.
37 P. J. Hagrman and J. Zubieta, *Inorg. Chem.*, 2000, **39**, 5218–5224.
38 P. Chaudhuri, K. Wieghardt, B. Nuber and J. Weiss, *J. Chem. Soc., Chem. Commun.*, 1987, 1198–1199.
39 K. Lettko, S. Liu and J. Zubieta, *Acta Crystallogr., Sect. C: Cryst. Struct. Commun.*, 1991, **47**, 1723–1725.
40 R. C. Holz, T. E. Elgren, L. L. Pearce, J. H. Zhang, C. J. O'Connor and L. Que, *Inorg. Chem.*, 1993, **32**, 5844–5850.
41 R. M. Davydov, J. Smieja, S. A. Dikanov, Y. Zang, L. Que Jr. and M. K. Bowman, *J. Biol. Inorg. Chem.*, 1999, **4**, 292–301.
42 J. Lu, C.-H. Lü, J.-H. Yu, J.-Q. Xu, Y. Li, X. Zhang, T.-G. Wang and Q.-X. Yang, *Polyhedron*, 2004, **23**, 755–761.
43 C.-H. Lü, J.-Q. Xu, J.-H. Yu, L. Ye, Y. Li, J. Lu, T.-G. Wang and J.-X. Cao, *Mendeleev Commun.*, 2003, **13**, 167–168.
44 A. Diebold and K. S. Hagen, *Inorg. Chem.*, 1998, **37**, 215–223.
45 A. L. Rheingold and J. R. Harper, *J. Organomet. Chem.*, 1991, **403**, 335–344.
46 C. Dinoi, G. Taban, P. Sözen, F. Demirhan, J.-C. Daran and R. Poli, *J. Organomet. Chem.*, 2007, **692**, 3743–3749.
47 A. S. Borovik, V. Papaefthymiou, L. F. Taylor, O. P. Anderson and L. Que, *J. Am. Chem. Soc.*, 1989, **111**, 6183–6195.
48 A. S. Borovik, M. P. Hendrich, T. R. Holman, E. Munck, V. Papaefthymiou and L. Que, *J. Am. Chem. Soc.*, 1990, **112**, 6031–6038.
49 S. Menage, Y. Zang, M. P. Hendrich and L. Que, *J. Am. Chem. Soc.*, 1992, **114**, 7786–7792.
50 Y. Zang and L. Que, *Inorg. Chem.*, 1995, **34**, 1030–1035.
51 I. Bertini, C. Luchinat and G. Parigi, *Solution NMR of paramagnetic molecules: Applications to metallobiomolecules and models*, Elsevier Science Ltd, Amsterdam and New York, 2001, vol. 2.
52 L. J. Ming, H. G. Jang and L. Que, *Inorg. Chem.*, 1992, **31**, 359–364.
53 I. Solomon, *Phys. Rev.*, 1955, **99**, 559–565.
54 Gerd N. La Mar, William DeW. Horrocks, Jr. and R. H. Holm, *NMR of paramagnetic molecules: Principles and applications*, Academic Press, New York, 1973.
55 C. S. Allen, C.-L. Chuang, M. Cornebise and J. W. Canary, *Inorg. Chim. Acta*, 1995, **239**, 29–37.
56 I. Bertini, C. Luchinat and D. Tarchi, *Chem. Phys. Lett.*, 1993, **203**, 445–449.
57 Z. Wang, T. R. Holman and L. Que, *Magn. Reson. Chem.*, 1993, **31**, S78–S84.
58 R. Çelenligil-Çetin, R. J. Staples and P. Stavropoulos, *Inorg. Chem.*, 2000, **39**, 5838–5846.
59 F. Meyer and H. Pritzkow, *Angew. Chem., Int. Ed.*, 2000, **39**, 2112–2115.
60 W. Micklitz, S. G. Bott, J. G. Bentsen and S. J. Lippard, *J. Am. Chem. Soc.*, 1989, **111**, 372–374.
61 K. Prout and J. C. Daran, *Acta Crystallogr., Sect. B: Struct. Crystallogr. Cryst. Chem.*, 1978, **34**, 3586–3591.
62 S. M. O. Quintal, H. I. S. Nogueira, H. M. Carapuça, V. Félix and M. G. B. Drew, *J. Chem. Soc., Dalton Trans.*, 2001, 3196–3201.
63 H. Liang, Z.-F. Chen, R.-X. Hu, Q. Yu, Z.-Y. Zhou and X.-G. Zhou, *Transition Met. Chem.*, 2002, **27**, 102–104.
64 T. J. Ahmed, L. N. Zakharov and D. R. Tyler, *Acta Crystallogr., Sect. E: Struct. Rep. Online*, 2008, **64**, m1370–m1371.
65 A. W. Addison, T. N. Rao, J. Reedijk, J. van Rijn and G. C. Verschoor, *J. Chem. Soc., Dalton Trans.*, 1984, 1349.
66 W. R. Roth and F. Hunold, *Liebigs Ann.*, 1995, **1995**, 1119–1122.
67 A. G. Davies and J. Lusztyk, *J. Chem. Soc., Chem. Commun.*, 1980, 554–555.
68 A. G. Davies and J. Lusztyk, *J. Chem. Soc., Perkin Trans. 2*, 1981, 692–696.
69 P. N. Culshaw, J. C. Walton, L. Hughes and K. U. Ingold, *J. Chem. Soc., Perkin Trans. 2*, 1993, 879–886.
70 G. M. Sheldrick, *Acta Crystallogr., Sect. A: Found. Crystallogr.*, 2008, **64**, 112–122.
71 A. L. Spek, *J. Appl. Crystallogr.*, 2003, **36**, 7–13.
72 Stoe & Cie, STOE X-RED, 1991.
73 D. F. Evans, *J. Chem. Soc.*, 1959, 2003.
74 G. A. Bain and J. F. Berry, *J. Chem. Educ.*, 2008, **85**, 532.
75 Z. Tyeklar, R. R. Jacobson, N. Wei, N. N. Murthy, J. Zubieta and K. D. Karlin, *J. Am. Chem. Soc.*, 1993, **115**, 2677–2689.
76 C. D. Abernethy, F. Bottomley, J. Chen, M. F. Kemp, T. C. Mallais and O. O. Womiloju, *Inorg. Synth.*, 1998, **32**, 207–214.
77 R. A. Heintz, J. A. Smith, P. S. Szalay, A. Weisgerber and K. R. Dunbar, *Inorg. Synth.*, 2002, **33**, 75–83.

78 D. Mandon, A. Machkour, S. Goetz and R. Welter, *Inorg. Chem.*, 2002, **41**, 5364–5372.
79 J. Sundermeyer, U. Radius and C. Burschka, *Chem. Ber.*, 1992, **125**, 2379–2384.
80 W. G. Klemperer and R. S. Liu, *Inorg. Chem.*, 1980, **19**, 3863–3864.
81 P. Dauban, L. Sanière, A. Tarrade and R. H. Dodd, *J. Am. Chem. Soc.*, 2001, **123**, 7707–7708.
82 M. R. Bukowski, P. Comba, A. Lienke, C. Limberg, C. L. de Laorden, R. Mas-Ballesté, M. Merz and L. Que Jr., *Angew. Chem. Int. Ed.*, 2006, **45**, 3446–3449.